https://doi.org/10.5194/egusphere-2026-4722
Preprint. Discussion started: 2 September 2026

Accuracy assessment of MODIS water vapor products in arid regions based on ground-based GNSS observations

Jiaxuan Sun[1,2], Yuwei Wu[1,2], Yuanzhu Zhang[1,2], Zaidong Liu[3]
[1]Shaanxi Key Laboratory of Earth Surface and Environmental Carrying Capacity, Xi'an, 710127, China
[2]College of Urban and Environmental Sciences, Northwest University, Xi'an, 710127, China
[3]Shanghai Huace Navigation Technology Co., Ltd., Shanghai, 201700, China

Correspondence to: Yuwei Wu (yuwei.wu@nwu.edu.cn)

Abstract. The MODIS precipitable water vapor (PWV) product has been widely used in hydrometeorological and hydro-ecological research because of its kilometer-scale spatial resolution, daily temporal resolution, and global coverage. However, its regional applicability, error characteristics, and correction methods remain insufficiently evaluated in arid regions because radiosonde (RS) stations are sparsely distributed and their routine observations at fixed times rarely coincide with MODIS overpasses. Based on RS observations and two Global Navigation Satellite System (GNSS) meteorological stations over the arid Hexi Corridor, we established a two-stage method in which fixed-time RS observations were first used to identify the most suitable GNSS-PWV retrieval scheme and correct the resulting estimates, after which the corrected GNSS-PWV series was used to evaluate MODIS-PWV at satellite overpass times. Results show that the GNSS-PWV retrievals were sensitive to weighted mean temperature (T_m) estimation, and those obtained using integrated T_m agreed better with RS-PWV. After RS-based linear correction, the corrected GNSS-PWV achieved R = 0.97 and RMSE = 2.30 mm. Relative to the corrected GNSS-PWV, MODIS-PWV showed a systematic overestimation, with mean biases of 2.21 mm at the reference station GSIA and 2.88 mm at the transfer-test station GSCM, and larger biases during high-PWV periods in summer. A univariate linear correction can effectively reduce the bias, with the RMSE decreasing from 3.47 to 2.05 mm at GSIA and from 5.22 to 3.58 mm at GSCM. This two-stage RS–GNSS–MODIS method provides a methodological reference for evaluating satellite-derived water vapor products and supporting their regional application in arid regions.

1 Introduction

Atmospheric water vapor is one of the most active components of the Earth's climate system, and its column-integrated amount is commonly expressed as precipitable water vapor (PWV). In addition to influencing the radiation budget through the greenhouse effect of water vapor, atmospheric water vapor regulates convective development, cloud microphysical processes, and precipitation efficiency through latent heat transport and phase changes, thereby exerting an important influence on the regional hydrological cycle and extreme precipitation events (Ding et al., 2022; Trenberth et al., 2005). Under global warming, the water-holding capacity of the atmosphere is expected to increase by approximately 7% for every 1 °C increase in air temperature (Miao et al., 2016). Numerous studies have shown that the spatiotemporal variation in atmospheric water vapor is closely associated with the acceleration of the hydrological cycle and the intensification of extreme precipitation (Allan and Soden, 2008; Held and Soden, 2006). Therefore, accurate and spatiotemporally continuous PWV information has become

https://doi.org/10.5194/egusphere-2026-4722
Preprint. Discussion started: 2 September 2026

essential for improving numerical weather prediction and supporting climate diagnosis and land–atmosphere interaction studies (Bai et al., 2025; Liu and Xia, 2010; Wu et al., 2021).

Among the available PWV observation and retrieval methods, radiosondes directly measure vertical atmospheric profiles. Microwave radiometers infer atmospheric water vapor from microwave emission and absorption, GNSS meteorology retrieves PWV from water-vapor-related signal propagation delays, and satellite near-infrared methods use water vapor absorption features in reflected solar radiation (Bevis et al., 1992; Zhao et al., 2018). Although RS observations are often treated as reference measurements, sounding stations are sparse and provide only twice-daily, discontinuous observations (Wang, 2018). The more recently developed GNSS meteorology technique overcomes the temporal sampling limitation with observation intervals as short as 30 seconds, providing all-weather, continuous, high-temporal resolution ground-based monitoring. It has thus become a key validation data source for satellite products (Wang et al., 2007). In terms of spatial coverage, both RS and GNSS provide station-scale information, whereas satellite remote sensing products can characterize the spatially continuous distribution of atmospheric water vapor over large areas. As a result, the integration of multisource satellite observations to produce PWV datasets with high spatial and temporal resolution has become an important research direction (Liu et al., 2025; Li et al., 2023; NASA/LARC/SD/ASDC, 2013). However, due to the differences in retrieval mechanisms for various water vapor products, inconsistencies and systematic biases still exist (Li et al., 2003). Therefore, ground-based accuracy assessment and bias correction of satellite water vapor products provide an important basis for their quantitative application and subsequent multisource integration.

Among satellite-derived water vapor products, the Moderate Resolution Imaging Spectroradiometer (MODIS), onboard the Terra and Aqua platforms, provides near-infrared PWV retrievals with relatively high spatial resolution and global coverage and has been widely used in weather process analysis, climate research, and hydro-ecological applications (Gao et al., 1993; Liu et al., 2006). The near-infrared algorithm retrieves column-integrated water vapor from the differential absorption of reflected solar radiation in water vapor absorption and atmospheric window bands near 0.940 µm (Kaufman and Gao, 1992; Gao and Goetz, 1990; Gao and Kaufman, 2003). Because this retrieval depends on reflected solar radiation, variations in surface spectral reflectance can affect the retrieved PWV, as examined by Wang et al. (2005). MODIS-PWV has also been used as an auxiliary product for atmospheric-delay correction in InSAR applications (Liu et al., 2007). As documented in numerous studies, the errors in MODIS-PWV are closely related to regional atmospheric moisture conditions, cloud conditions, and underlying surface characteristics and consequently exhibit marked regional and seasonal differences (Liu et al., 2026; Lu et al., 2011; Zhu et al., 2021). According to an error evaluation based on 246 GNSS stations across China, there is a systematic overestimation of MODIS-PWV relative to GNSS, with larger biases under humid summer conditions (Zhu et al., 2021), which is reported to have an error range from 3 to 6 mm across different regions (Zhao et al., 2022). Arid regions are characterized by low atmospheric water vapor content, but existing studies often evaluate errors across the entire Northwest China or even combine it with the Tibetan Plateau, leaving considerable uncertainty regarding the representativeness of the reported errors for typical arid environments. Moreover, although several correction approaches, including linear regression, regional correction, and machine-learning methods, have been proposed for MODIS-PWV (Liu et al., 2026; Xiong et al., 2021; Ghaderi

https://doi.org/10.5194/egusphere-2026-4722
Preprint. Discussion started: 2 September 2026

and Rahimzadegan, 2022), local ground-based validation and applicability assessments specifically targeting arid regions remain limited.

Due to sparse RS stations and difficulty in matching the RS data with satellite overpasses, many previous studies have directly used GNSS-derived PWV as the reference for evaluating MODIS-PWV, so residual errors in the GNSS retrieval may be propagated into the MODIS-PWV assessment. To address this, we focus on the Hexi Corridor, a typical arid region with publicly available RS observations, and use RS-PWV to identify the GNSS-PWV retrieval method suitable for this region; the resulting optimal GNSS-PWV is then adopted as the reference for evaluating MODIS-PWV. In this study, we compared two widely used GNSS processing methods, including the precise point positioning (PPP) and regional network processing based on GAMIT/GLOBK (hereafter GAMIT). For weighted mean temperature (T_m) estimation, in addition to the conventional Bevis empirical model, T_m was calculated by vertical integration of ERA5 temperature and humidity profiles to reduce the potential errors associated with the Bevis model in arid environments (Cui et al., 2025). Accordingly, this study has three specific objectives: (1) to identify the combination of GNSS processing strategy (PPP or GAMIT) and T_m estimation method (the Bevis empirical model or ERA5 profile integration) that yields the most reliable PWV estimates in arid environments under limited RS observations; (2) to quantify the magnitude, direction, and seasonality of MODIS-PWV errors over the Hexi Corridor; and (3) to develop a region-specific correction model and evaluate its effectiveness and transferability in reducing MODIS-PWV errors under similar arid conditions. Through this two-stage RS–GNSS–MODIS method, this study provides a methodological reference for evaluating and correcting satellite-derived water vapor products in arid regions, particularly in areas where GNSS stations exist but radiosonde observations are unavailable.

2 Data and methods

2.1 Study area

The study area is located in the western Hexi Corridor of Gansu Province, within the inland arid region of northwestern China (Fig. 1). Because it is far from oceanic moisture sources, the region has a typical temperate continental arid climate, characterized by scarce precipitation, strong evaporation, and generally low atmospheric water vapor content (Yu et al., 2017; Zhang et al., 2015). The underlying surface is dominated by Gobi, desert, and bare rock, with sparse vegetation and relatively high surface reflectance, making the region representative of the arid land-surface environment of northwestern China (Luo et al., 2012; Zheng et al., 2015). The combination of low atmospheric water vapor content and a high-albedo surface provides a suitable setting for evaluating the applicability of MODIS-PWV in arid regions.

Two GNSS stations are located within the study area: GSIA (39.794° N, 98.327° E) and GSCM (39.851° N, 96.766° E). GSIA is located near the Jiuquan radiosonde station, allowing time-matched GNSS-PWV and RS-PWV observations to be obtained; it was therefore selected as the reference station. GSCM, which lacks collocated radiosonde observations, was used as a transfer-test site to evaluate the established relationship between GNSS-PWV (calibrated with the reference station) and MODIS-PWV.

https://doi.org/10.5194/egusphere-2026-4722
Preprint. Discussion started: 2 September 2026

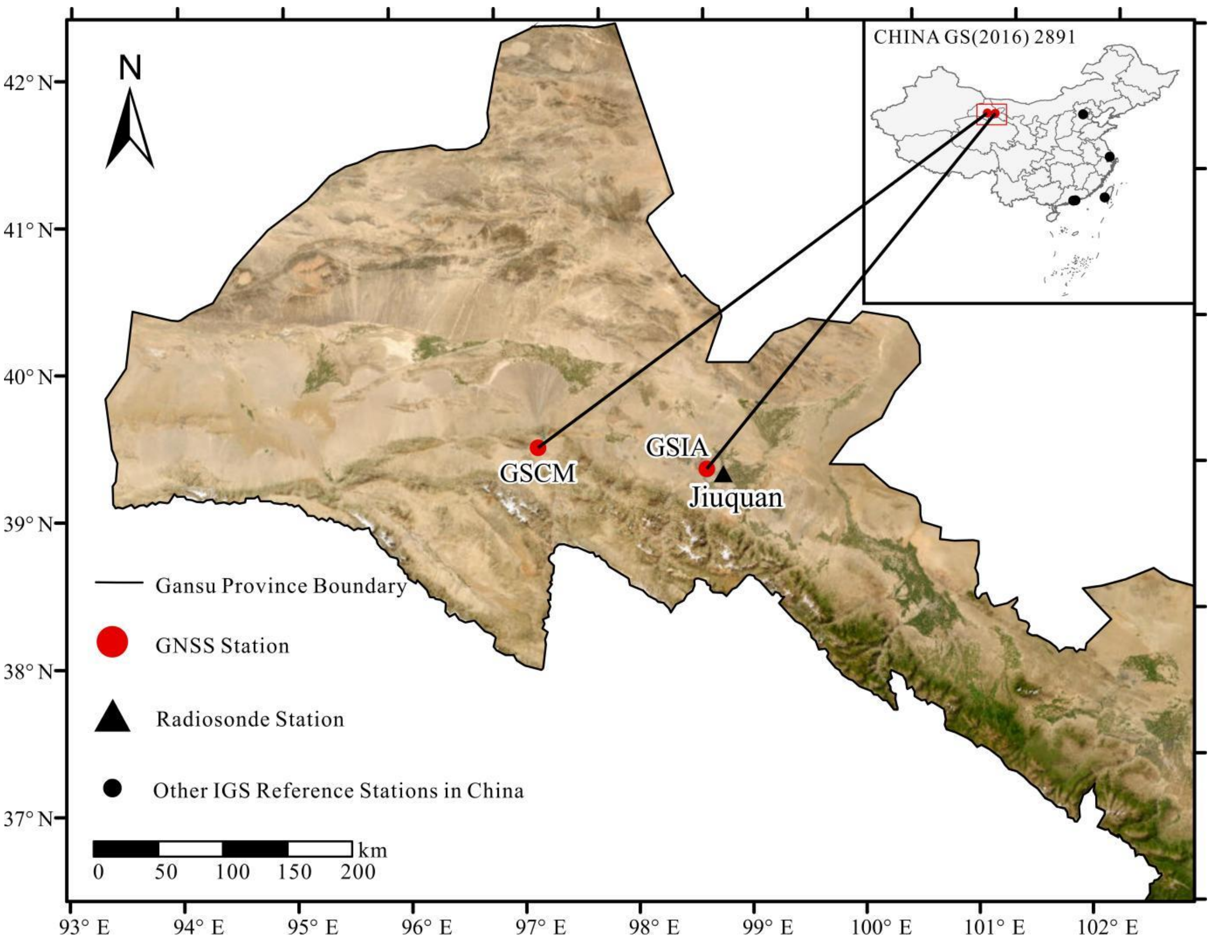

Figure 1: Location map of study area and distribution of ground-based observation stations.

Basemap: ArcGIS World Imagery (Source: Esri, Vantor, Earthstar Geographics, and the GIS User Community). Map lines delineate study areas and do not necessarily depict accepted national boundaries.

2.2 Data

2.2.1 Ground-based GNSS observations

Both GNSS stations collected data from 1 September 2024 to 31 August 2025, encompassing a complete annual cycle of atmospheric water vapor variation. Both stations were equipped with dual-frequency Huace H6 GNSS receivers, providing continuous observations at a sampling interval of 30 s. The raw observations were subjected to basic quality control and format conversion using TEQC (Translation, Editing, and Quality Checking), during which data gaps and cycle slips were checked and epochs with low signal-to-noise ratios or pronounced multipath effects were removed. The resulting clean data were then used as input for the subsequent tropospheric delay estimation.

https://doi.org/10.5194/egusphere-2026-4722
Preprint. Discussion started: 2 September 2026

2.2.2 Radiosonde observations

The Jiuquan upper-air radiosonde station is adjacent to GSIA (data available from: https://weather.uwyo.edu/upperair/sounding.shtml). Radiosondes are launched twice daily at 00:00 and 12:00 UTC, providing vertical profiles of pressure, temperature, dew-point temperature, and other meteorological variables from the surface to the upper atmosphere. PWV was calculated by integrating the sounding profiles and was used to evaluate the accuracy of GNSS-PWV retrieved using the PPP and GAMIT methods.

Based on the radiosonde profiles, PWV was calculated as follows (Zhang et al., 2019):

$$\mathrm{PWV}=\frac{1}{\rho_{\omega}}\int_{\mathrm{p_t}}^{\mathrm{p_s}}\frac{\mathrm{q(p)}}{\mathrm{g(p)}}\mathrm{dp} \quad , \tag{1}$$

where ρ_{ω} is the density of liquid water (1000 kg m^{-3}); q(p) and g(p) are the specific humidity (kg kg^{-1}) and gravitational acceleration (m s^{-2}) at pressure p, respectively; and pt and p_s are the pressures at the profile top and surface, respectively. The integral was evaluated using the trapezoidal rule, and PWV was converted to millimeters.

2.2.3 ERA5 reanalysis data

To obtain surface pressure at the GNSS stations, the ERA5 hourly data on single levels provided by the European Centre for Medium-Range Weather Forecasts (ECMWF) were used (Hersbach et al., 2018a). The data have a horizontal resolution of 0.25° × 0.25°. The single-level variables included surface pressure (sp) and surface geopotential (z). Surface geopotential was converted to geopotential height using H = z/g, and the resulting grid-point height was used together with the GNSS-station elevation to adjust the interpolated surface pressure. The adjusted station-level surface pressure was then used in the Saastamoinen model to calculate zenith hydrostatic delay (ZHD).

In addition, the ERA5 hourly data on pressure levels were used to obtain air temperature, specific humidity, and geopotential at multiple levels (Hersbach et al., 2018b). These variables were used to calculate T_m by vertical integration, which was subsequently used to determine the water vapor conversion factor in the GNSS-PWV retrieval.

2.2.4 MODIS satellite remote sensing data

The MODIS, onboard the Terra and Aqua satellite platforms, provides global multispectral observations with high spatial resolution and daily temporal coverage. This study used the Terra/MODIS Level-2 precipitable water vapor product MOD05, together with the MOD03 geolocation product and the MOD35 cloud-mask product, for the spatial positioning, cloud screening, and station matching of MODIS-PWV. All datasets were obtained from the NASA LAADS DAAC platform (available at: https://ladsweb.modaps.eosdis.nasa.gov/search).

MOD05 is the MODIS Near-Infrared Total Precipitable Water Product (MODIS Atmosphere Science Team, 2017a), with a spatial resolution of 1 km × 1 km, and provides atmospheric water vapor retrievals at Terra overpass times. Based on the radiometrically calibrated MOD021KM product, MOD05 retrieves the PWV using radiance information from water vapor absorption bands (the 0.940 μm) and adjacent atmospheric window bands. A channel-ratio method is used to reduce the influence of surface reflectance and retrieve tropospheric precipitable water vapor.

https://doi.org/10.5194/egusphere-2026-4722
Preprint. Discussion started: 2 September 2026

MOD03 is the MODIS Geolocation Fields Product and is generated simultaneously with the spectral observations (MODIS Science Data Support Team, 2017). It provides pixel-level latitude, longitude, and observation geometry, including the sensor viewing angle, solar zenith angle, and solar azimuth angle, at a spatial resolution corresponding to MOD05. In this study, MOD03 was used to determine the precise geographic locations and observation geometry of MOD05 pixels, providing the basis for station-centered spatial-window extraction and spatiotemporal matching.

MOD35 is the MODIS Cloud Mask Product (MODIS Atmosphere Science Team, 2017b), which evaluates the cloud condition of each pixel through a series of decision tests based on multispectral brightness temperatures and reflectance characteristics, together with spatial texture and observation geometry. It classifies each determined pixel into four confidence levels according to the unobstructed field-of-view quality flag: confident cloudy, probably cloudy, probably clear, and confident clear. In this study, MOD35 was used to establish a clear-sky screening criterion in which pixels classified as probably clear or confident clear were retained. By matching the MOD35 cloud-mask fields with MOD05 on a pixel-by-pixel basis, pixels affected by clouds were removed, thereby reducing PWV underestimation or retrieval distortion when cloud-top reflectance dominates the observed radiance signal.

2.3 Data processing and methods

2.3.1 Tropospheric delay estimation and PWV retrieval

For tropospheric delay estimation, two commonly used GNSS processing methods were applied independently to estimate zenith total delay (ZTD): precise point positioning (PPP) and regional network processing based on GAMIT. In the PPP approach, observations from each GNSS station were processed independently using precise satellite orbit and clock products, and the station coordinates, receiver clock offsets, carrier-phase ambiguities, and ZTD were estimated simultaneously. By contrast, GAMIT combined the stations in the study area with several reference stations to form a regional network and derived the ZTD time series through joint adjustment.

The quality-controlled GNSS observations sampled at 30 s intervals were processed separately using PPP and GAMIT. ZTD was estimated at 1 h intervals, producing an hourly ZTD time series. ZTD was then separated into zenith hydrostatic delay (ZHD) and zenith wet delay (ZWD) (Shen, 2018):

$$ZTD = ZHD + ZWD, \tag{2}$$

ZHD was calculated using the Saastamoinen model (Saastamoinen, 1973):

$$ZHD = 0.0022768 \frac{P_s}{1\text{-}0.00266\ \cos(2\varphi)\ \text{-}0.00028H}, \tag{3}$$

where Ps is the surface pressure at the station (hPa), φ is latitude, and H is station elevation (km). Surface pressure for the ZHD calculation was obtained from ERA5 single-level data through spatial interpolation and elevation adjustment.

After ZWD was obtained, it was converted to PWV using T_m and the water vapor conversion factor (Π):

$$PWV=\Pi \times ZWD, \tag{4}$$

https://doi.org/10.5194/egusphere-2026-4722
Preprint. Discussion started: 2 September 2026

$$\Pi=\frac{1\times10^{6}}{\rho R_v[(\frac{k_3}{T_m}+k_2')]}, \quad (5)$$

where Π is the water vapor conversion factor related to T_m, serving as a critical parameter for mapping the wet delay into water vapor mass. ρ represents the density of liquid water (1000 kg m^{-3}), and R_v = 0.462 J g^{-1} K^{-1} and R_d = 0.287 J g^{-1} K^{-1} are the specific gas constants for water vapor and dry air, respectively. The atmospheric refractivity constants are k_1 = 77.604 K hPa^{-1}, k_2 = 64.790 K hPa^{-1}, k_3 = 3.776 × 105 K^2 hPa^{-1}, $k_2' = k_2 - k_1\frac{R_d}{R_v}$.

2.3.2 Estimation of weighted mean temperature

Weighted mean temperature (T_m) is a key intermediate physical variable in the conversion of zenith wet delay into PWV and represents the vertically weighted temperature state of atmospheric water vapor. Two methods were compared to estimate T_m. The first method was the Bevis empirical model, in which T_m is approximated as a linear function of surface air temperature (T_s):

$$T_m = 70.2 + 0.72T_s, \quad (6)$$

However, the vertical temperature structure in arid regions is relatively complex, and surface temperature may differ substantially from the weighted temperature of the atmospheric column. This empirical relationship may therefore introduce systematic bias under such conditions (Wang et al., 2016; Xie et al., 2025), producing occasional extreme outliers in the GNSS-PWV estimates.

The second method used the vertical profiles of temperature and specific humidity provided by the ERA5 pressure-level data to calculate T_m through discrete integration according to its physical definition. The water vapor conversion factor Π was then recalculated using the resulting integrated T_m. The atmospheric column was divided into multiple layers, and T_m was calculated as follows:

$$T_m = \frac{\sum_k \frac{e_k}{T_k}\Delta z_k}{\sum_k \frac{e_k}{T_k^2}\Delta z_k}, \quad (7)$$

where T_k, ek, and Δz_k are the temperature, water vapor pressure, and thickness of the k-th atmospheric layer, respectively. In practice, the ek at each pressure level was calculated from the ERA5 temperature and specific humidity data. Vertical integration was then performed to obtain T_m for each station and observation time, which were used to calculate Π and retrieve GNSS-PWV.

2.3.3 MODIS data preprocessing and spatiotemporal collocation

Because the near-infrared water vapor absorption bands are sensitive to atmospheric conditions and cloud cover, the MODIS near-infrared PWV algorithm is mainly applicable under daytime clear-sky or near-clear-sky conditions. Cloud screening was therefore required before evaluating MODIS-PWV. Following previous studies, orbital images with high overall cloud-free fractions were prioritized, and MOD05 retrievals were included in the analysis only under locally near-clear-sky conditions.

https://doi.org/10.5194/egusphere-2026-4722
Preprint. Discussion started: 2 September 2026

The MOD05, MOD03, and MOD35 products were jointly used to preprocess and spatiotemporally match the MODIS-PWV over the study area. First, the three products from the same satellite overpass were co-registered to ensure strict pixel-level correspondence. The cloud-detection results from MOD35 were then used to remove pixels classified as "confident cloudy" or "probably cloudy". Only pixels classified as "confident clear" or "probably clear" were retained as valid samples for comparison between MODIS-PWV and GNSS-PWV (Xu, 2022).

After quality control, each Terra overpass time was used as the temporal reference. GNSS-PWV values within ±30 min of the overpass were selected from the hourly GNSS-PWV series corrected using RS-PWV and used as the corresponding ground-based reference. For spatial matching, following Bai et al. (2021), a fixed 31 km × 31 km window centered on each GNSS station was adopted. The mean PWV of all MOD05 pixels within the window that satisfied the cloud-screening criteria was calculated as the station-matched MODIS-PWV. The resulting matched dataset was used for the subsequent accuracy assessment and linear correction of MODIS-PWV in the arid study area.

2.3.4 Statistical metrics for accuracy assessment

To evaluate the differences among the PWV datasets and the effects of correction, the Pearson correlation coefficient (R), root mean square error (RMSE), mean bias (Bias), and standard deviation of the differences (STD) were used as accuracy metrics. Let xi denotes the PWV value to be evaluated, yi is the corresponding reference PWV value, and N the number of paired samples. The symbols $\bar{x}$ and $\bar{y}$ denote the sample means of xi and yi, respectively. The metrics were calculated as follows:

Pearson correlation coefficient:

$$R=\frac{\sum_{i=1}^{N}(x_i-\bar{x})(y_i-\bar{y})}{\sqrt{\sum_{i=1}^{N}(x_i-\bar{x})^2}\sqrt{\sum_{i=1}^{N}(y_i-\bar{y})^2}}, \tag{8}$$

Root mean square error:

$$RMSE=\sqrt{\frac{1}{N}\sum_{i=1}^{N}(x_i-y_i)^2}, \tag{9}$$

Mean bias:

$$Bias=\frac{1}{N}\sum_{i=1}^{N}(x_i-y_i), \tag{10}$$

Standard deviation of the differences:

$$STD=\sqrt{\frac{1}{N-1}\sum_{i=1}^{N}[(x_i-y_i)-Bias]^2}, \tag{11}$$

2.3.5 Linear correction of GNSS-PWV constrained by RS-PWV

Because GSIA is adjacent to the Jiuquan radiosonde station, RS-PWV was used as a reference for GNSS-PWV correction at this site. A univariate linear correction model was established using the temporally matched RS-PWV and GNSS-PWV samples:

$$PWV_{GNSS,corr}=a_G \cdot PWV_{GNSS,raw}+b_G, \tag{12}$$

https://doi.org/10.5194/egusphere-2026-4722
Preprint. Discussion started: 2 September 2026

where $PWV_{GNSS,raw}$ and $PWV_{GNSS,corr}$ are the raw and corrected GNSS-PWV values, respectively, and a_G and b_G are the slope and intercept, respectively. Bias, RMSE, STD, and R were calculated for both the raw and corrected GNSS-PWV series relative to RS-PWV.

When RS-corrected GNSS-PWV is subsequently used as the reference, these metrics characterize the relative errors of the evaluated data with respect to the transfer reference rather than their absolute errors relative to RS-PWV. The accuracy assessment of MODIS-PWV therefore also requires an error propagation analysis that accounts for the residual errors in the corrected GNSS-PWV series.

Because no radiosonde data are available near GSCM, a site-specific RS-PWV-constrained correction model was not established at this station. Instead, the correction relationship derived at GSIA was applied to GSCM to generate a corrected GNSS-PWV series under the same regional conditions and retrieval method. The resulting series was subsequently used to compare the relative errors of MODIS-PWV before and after correction and to assess the transferability of the correction model.

2.3.6 MODIS-PWV correction and error propagation assessment

Radiosonde observations were available only at fixed launch times, whereas MODIS-PWV was obtained at satellite overpass times. Because the observation times did not coincide, MODIS-PWV could not be directly validated against synchronous RS-PWV. The RS-corrected GNSS-PWV series was therefore used as a transfer reference for evaluating and correcting MODIS-PWV.

Using the corrected GNSS-PWV as the reference and raw MODIS-PWV as the predictor, a univariate linear correction model was established:

$$PWV_{MODIS,corr}=a_M \cdot PWV_{MODIS,raw}+b_M, \tag{13}$$

where $PWV_{MODIS,raw}$ and $PWV_{MODIS,corr}$ are the raw and corrected MODIS-PWV values, respectively, and a_M and b_M are the slope and intercept.

Given that residual cloud contamination, local variations in surface reflectance, and spatiotemporal collocation errors can cause anomalous deviations in some paired samples, to reduce their influence on the fitted parameters, the difference (ΔPWV) between raw MODIS-PWV and corrected GNSS-PWV at GSIA was defined as:

$$\Delta PWV = PWV_{MODIS,raw} - PWV_{GNSS,corr}, \tag{14}$$

Paired samples outside the $\mu \pm 3\sigma$ range were treated as outliers, where μ and σ are the mean and standard deviation of ΔPWV, respectively. The final correction equation was established using all remaining valid GSIA samples. The same $\mu \pm 3\sigma$ criterion was applied to identify anomalous validation samples at GSCM.

Because the corrected GNSS-PWV still contains residual error relative to RS-PWV, the absolute error of MODIS-PWV with respect to true reference includes not only its errors relative to corrected GNSS-PWV, but also the residual error of corrected GNSS-PWV relative to RS-PWV. The propagated biases of raw and corrected MODIS-PWV were calculated as:

$$Bias_{MODIS,abs,raw}=Bias_{MODIS,rel,raw}+Bias_{GNSS,corr}, \tag{15}$$

$$\mathrm{Bias}_{\mathrm{MODIS,abs,corr}}=\mathrm{Bias}_{\mathrm{MODIS,rel,corr}}+\mathrm{Bias}_{\mathrm{GNSS,corr}}, \tag{16}$$

Similarly, the corresponding propagated RMSE values were estimated as:

$$\mathrm{RMSE}_{\mathrm{MODIS,abs,raw}}=\sqrt{\mathrm{RMSE}^2_{\mathrm{MODIS,rel,raw}}+\mathrm{RMSE}^2_{\mathrm{GNSS,corr}}}, \tag{17}$$

$$\mathrm{RMSE}_{\mathrm{MODIS,abs,corr}}=\sqrt{\mathrm{RMSE}^2_{\mathrm{MODIS,rel,corr}}+\mathrm{RMSE}^2_{\mathrm{GNSS,corr}}}, \tag{18}$$

where $\mathrm{Bias}_{\mathrm{MODIS,rel,raw}}$ and $\mathrm{RMSE}_{\mathrm{MODIS,rel,raw}}$ denote the relative bias and RMSE of raw MODIS-PWV against corrected GNSS-PWV, respectively; $\mathrm{Bias}_{\mathrm{MODIS,rel,corr}}$ and $\mathrm{RMSE}_{\mathrm{MODIS,rel,corr}}$ mean the corresponding quantities after MODIS-PWV correction. $\mathrm{Bias}_{\mathrm{GNSS,corr}}$ and $\mathrm{RMSE}_{\mathrm{GNSS,corr}}$ are the residual bias and RMSE of corrected GNSS-PWV relative to RS-PWV, respectively. The propagated RMSE provides an approximate radiosonde-referenced error estimate because synchronous RS-PWV observations at exact MODIS overpass times are unavailable and the covariance term cannot be determined for individual matched samples. Propagated absolute bias (Abs Bias) and absolute root mean square error (Abs RMSE) were calculated only for GSIA. At GSCM, where no independent RS-PWV observations are available, only R, RMSE, STD, and Bias relative to corrected GNSS-PWV were calculated before and after MODIS-PWV correction to assess the relative correction performance after model transfer.

3 Results

3.1 Selection of the GNSS-PWV retrieval scheme

At the reference station GSIA, GNSS-PWV was estimated separately using both PPP and GAMIT methods, and the retrievals were validated against RS-PWV from Jiuquan radiosonde station as the reference. Each of the two retrieval methods was also combined with two T_m estimation approaches, resulting in a total of four combination schemes. These schemes were compared to evaluate their applicability under arid conditions.

3.1.1 Comparison of PPP and GAMIT under the Bevis-T_m scheme

Comparison of GNSS-PWV retrievals using PPP and GAMIT under the Bevis-T_m scheme with RS-PWV at GSIA showed better agreements for the GAMIT/Bevis scheme with RS-PWV than the PPP/Bevis scheme (Fig. 2). Although the Bias values of both schemes were close to zero, indicating no evident overall systematic bias, the residual time series showed several large outlying residuals for PPP/Bevis under moderate PWV conditions. The GAMIT/Bevis combination scheme showed better linear agreement with the observations, with a correlation coefficient of 0.94 and both RMSE and STD of approximately 3.4 mm. The linear fitting results also indicated that this scheme was more suitable for subsequent correction, as its residuals were more concentrated across both low- and high-PWV ranges, demonstrating better overall stability.

https://doi.org/10.5194/egusphere-2026-4722
Preprint. Discussion started: 2 September 2026

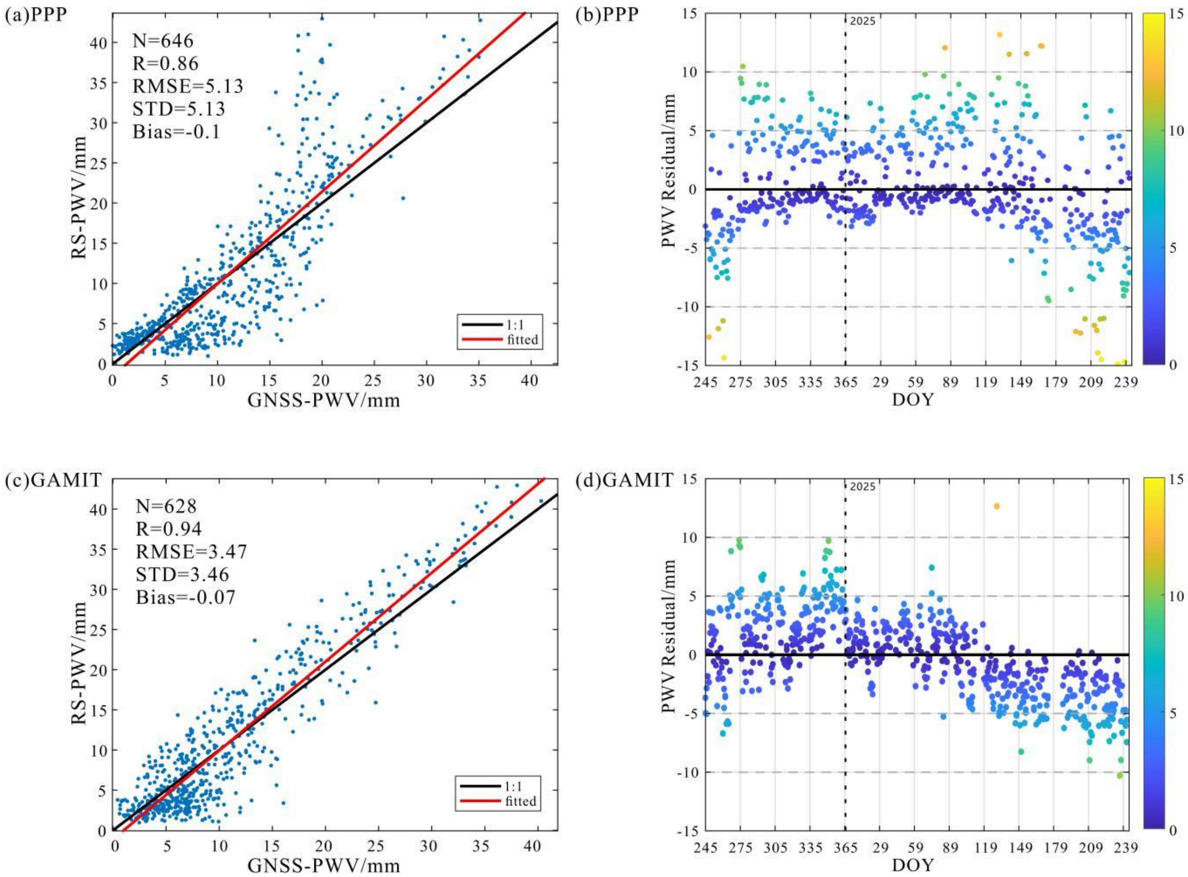

Figure 2: Comparison of GNSS-PWV and RS-PWV at GSIA under the Bevis-T_m scheme: (a) scatterplot and fitted line for PPP; (b) residual time series for PPP; (c) scatterplot and fitted line for GAMIT; and (d) residual time series for GAMIT.

3.1.2 Comparison of PPP and GAMIT under the integrated T_m scheme

To reduce the potential parameterization errors introduced by the Bevis-T_m model under arid conditions, T_m was further calculated according to its physical definition by integrating vertically, based on which the water vapor conversion factor was recalculated. Comparison between the RS-PWV and the GNSS-PWV retrieved by PPP and GAMIT under integrated T_m scheme shows that (Figs. 3a–b) the PPP/integrated-T_m scheme produced better retrieval results than the PPP/Bevis-T_m scheme. The correlation coefficient increased to 0.97, while RMSE and STD were 3.89 and 2.49 mm, respectively, indicating that the incorporation of integrated T_m can substantially reduce the errors of the PPP-derived PWV estimates. Although GNSS-PWV showed an overall underestimation relative to RS-PWV (with a Bias of −2.99 mm), the fitted relationship indicated marked improvement in terms of both consistency and stability of the estimates across the entire range of PWV.

https://doi.org/10.5194/egusphere-2026-4722
Preprint. Discussion started: 2 September 2026

By contrast, the GAMIT/integrated-T_m scheme (Figs. 3c–d) exhibited no evident improvement in the statistical metrics compared with the GAMIT/Bevis scheme, indicating that the influence of integrated T_m differed between the two GNSS processing methods. For PPP, the use of integrated T_m substantially increased the correlation with RS-PWV and reduced both random errors and residual dispersion; for GAMIT, however, the results obtained using integrated T_m showed little difference from those obtained using Bevis-T_m.

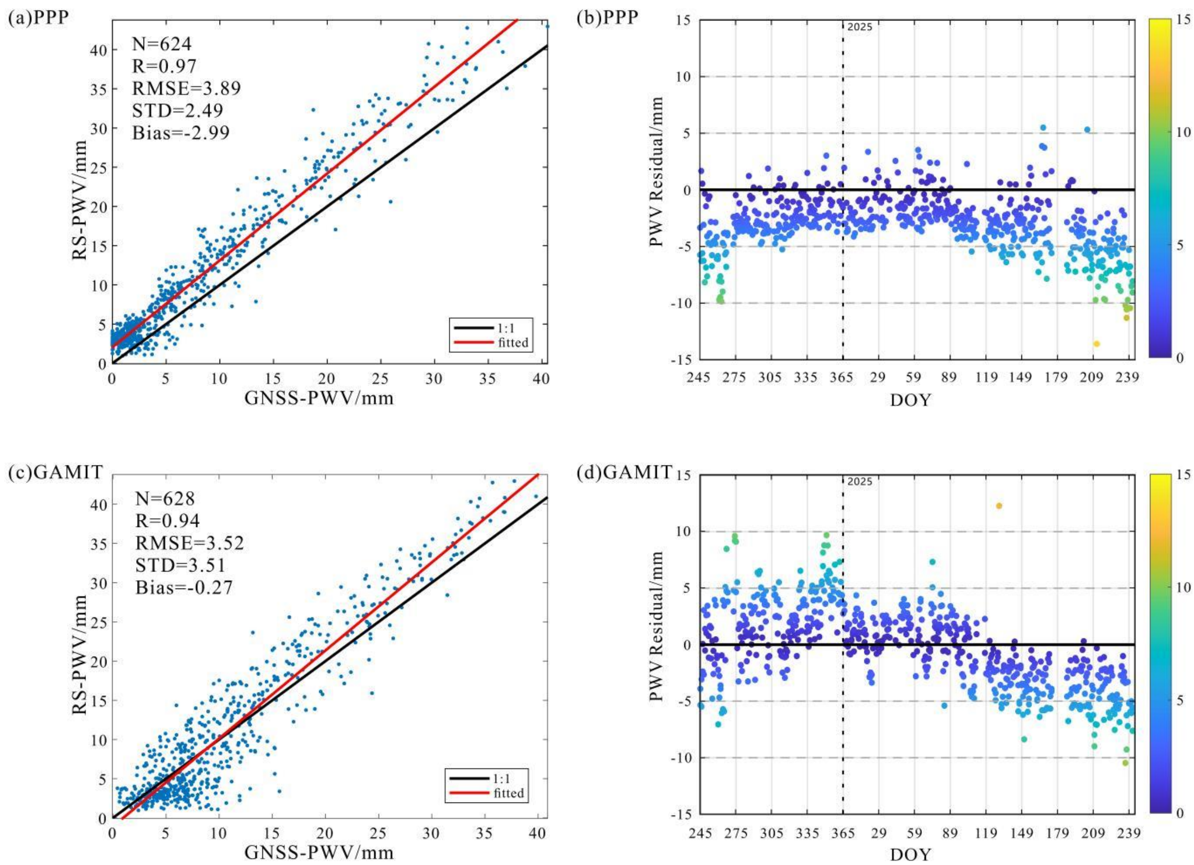

Figure 3: Comparison of GNSS-PWV and RS-PWV at GSIA under the integrated T_m scheme: (a) scatterplot and fitted line for PPP; (b) residual time series for PPP; (c) scatterplot and fitted line for GAMIT; and (d) residual time series for GAMIT.

3.2 Establishment of the corrected GNSS-PWV series

Comparison of the four combination schemes at the GSIA station showed that, in terms of both accuracy metrics and the overall residual distribution, the PPP/integrated-T_m scheme had the best overall accuracy and linear correction conditions. Therefore, the RS-PWV was used to linearly correct the GNSS-PWV estimates obtained using this scheme, so as to produce an RS-constrained corrected GNSS-PWV and to analyze the errors changes before and after correction. On this basis, the

https://doi.org/10.5194/egusphere-2026-4722
Preprint. Discussion started: 2 September 2026

corresponding correction relationship was further applied to the GSCM station, where no radiosonde observations were available, to construct a corrected GNSS-PWV series for this station.

Based on the temporally matched RS-PWV samples and GNSS-PWV estimates obtained using the PPP/integrated-T_m scheme at GSIA, the following linear correction equation was established:

$$PWV_{GNSS,corr} = 1.107 \cdot PWV_{GNSS,raw} + 2.057, \quad (19)$$

After linear correction using RS-PWV, variations in GNSS-PWV showed good agreement with those in RS-PWV (Fig. 4a), and the systematic pre-correction underestimation was substantially reduced. The scatterplot further showed that the corrected points moved markedly closer to the 1:1 line (Fig. 4b), with Bias decreased from −2.99 to 0.00 mm, RMSE decreased from 3.89 to 2.30 mm, and STD decreased to 2.30 mm. The corrected series thus provided a suitable reference for the subsequent evaluation and correction of MODIS-PWV at GSIA. For GSCM, where radiosonde observations were unavailable, the correction equation derived at GSIA was applied to the original GNSS-PWV retrievals, producing an RS-constrained corrected GNSS-PWV series for the subsequent evaluation of MODIS-PWV at GSCM.

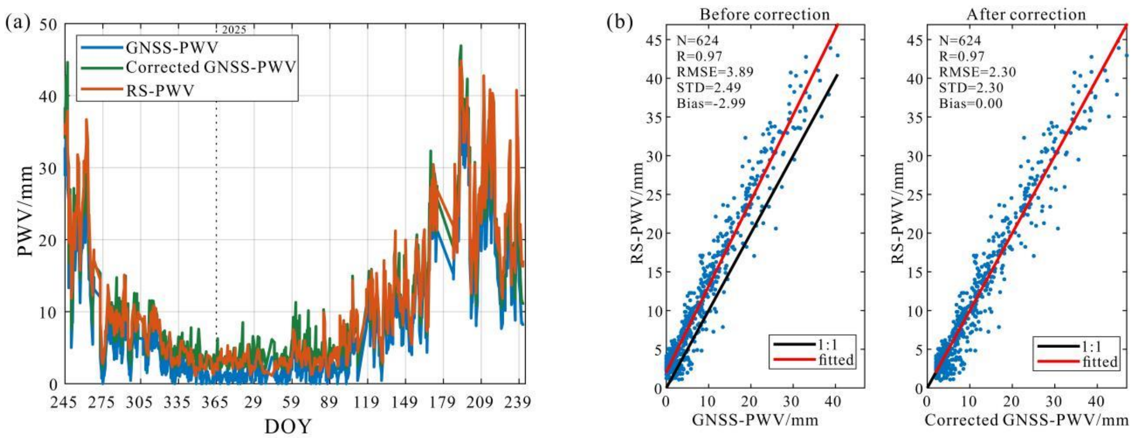

Figure 4: Comparison of GNSS-PWV before and after correction at GSIA using the PPP/integrated-T_m scheme: (a) time series; and (b) scatterplots and fitted lines before and after correction.

3.3 Accuracy assessment of MODIS-PWV in the arid study area

After the corrected GNSS-PWV series had been constructed, the error characteristics of MODIS-PWV in the arid region were further evaluated. To reduce the influence of individual outlying matched samples on the accuracy statistics, outliers were removed using the $\mu \pm 3\sigma$ criterion based on the differences between MODIS-PWV and corrected GNSS-PWV. All subsequent accuracy assessments and linear corrections were conducted using the valid samples after outlier removal.

As shown in Fig. 5, MODIS-PWV generally captured the intra-annual variations in PWV at both stations, with the timing of high and low PWV periods and most episodic fluctuations broadly consistent with the ground-based reference series. However, MODIS-PWV was generally higher than the reference series, and the residual dispersion tended to increase under higher PWV

https://doi.org/10.5194/egusphere-2026-4722
Preprint. Discussion started: 2 September 2026

conditions. The mean biases were 2.21 mm at GSIA and 2.88 mm at GSCM, with corresponding RMSE values of 3.47 and 5.22 mm, respectively (Fig. 5). The other statistical metrics are shown in Fig. 5. After accounting for the residual error in the corrected GNSS-PWV and its propagation, the Abs RMSE at GSIA was 4.16 mm. The results at the GSIA station indicate that MODIS-PWV can track the temporal variation in total column water vapor over the arid Hexi Corridor but still shows systematic overestimation relative to the RS-constrained reference. This positive bias is also confirmed at GSCM under similar arid conditions.

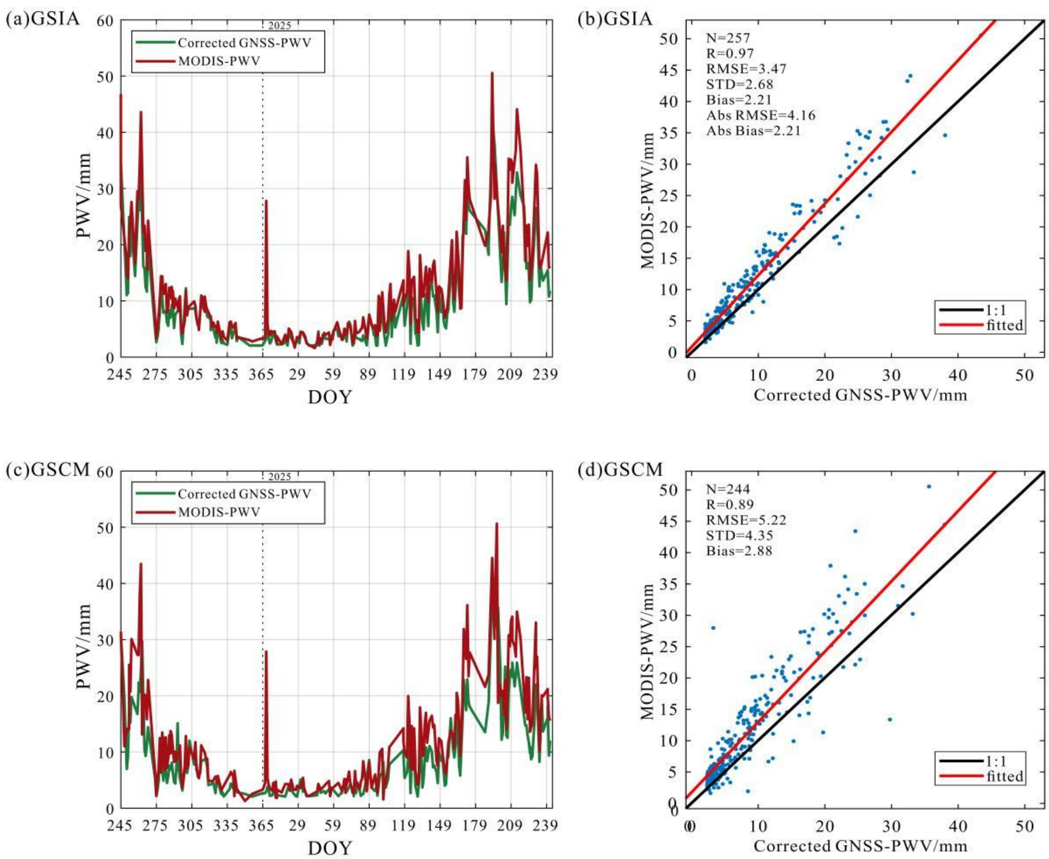

Figure 5: Comparison of MODIS-PWV and corrected GNSS-PWV: (a) time series at GSIA; (b) scatterplot and fitted line at GSIA; (c) time series at GSCM; and (d) scatterplot and fitted line at GSCM.

3.4 Correction of MODIS-PWV based on the corrected GNSS-PWV series

Using the corrected GNSS-PWV series as the reference, a linear correction equation for MODIS-PWV was first established from the valid GSIA samples after removal of the 3σ outliers. The equation was then applied to GSCM to examine the

https://doi.org/10.5194/egusphere-2026-4722
Preprint. Discussion started: 2 September 2026

applicability of the statistical relationship under the same regional conditions. The linear correction equation for MODIS-PWV is given as follows:

$$PWV_{MODIS,corr} = 0.817 \times PWV_{MODIS,raw} - 0.071, \quad (20)$$

After correction, both the RMSE and STD of MODIS-PWV relative to the corrected GNSS-PWV decreased to 2.05 mm, with Bias reduced to 0.00 mm (Fig. 6). The corrected samples moved markedly closer to the 1:1 line, and the residual distribution also improved substantially. These results show that the univariate linear model effectively reduced the systematic bias and the overall error level. The correction equation established at GSIA was further applied to GSCM (Fig. 7). After correction, Bias decreased from 2.88 to 0.62 mm, RMSE decreased from 5.22 to 3.58 mm, and STD decreased from 4.35 to 3.53 mm. Taken together, the results from GSIA and GSCM show that the univariate linear model established using the corrected GNSS-PWV series can effectively reduce the systematic overestimation of MODIS-PWV and improve its agreement with ground-based water vapor observations to some extent. The statistical relationship derived at GSIA remained applicable under similar arid conditions.

https://doi.org/10.5194/egusphere-2026-4722
Preprint. Discussion started: 2 September 2026

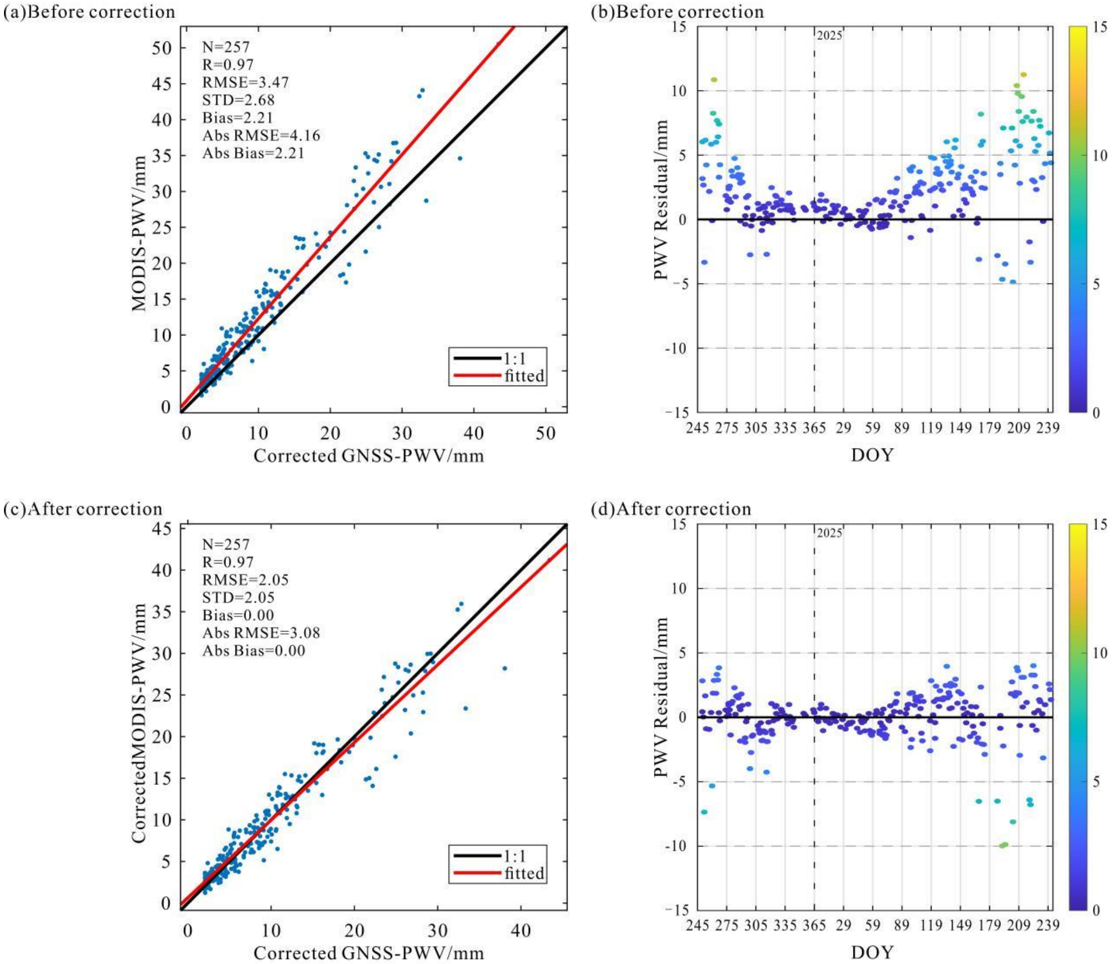

Figure 6: Comparison of MODIS-PWV with corrected GNSS-PWV at GSIA (Top) before and (Bottom) after linear correction:
365 (Left) scatterplot and fitted line and (Right) their residual time series.

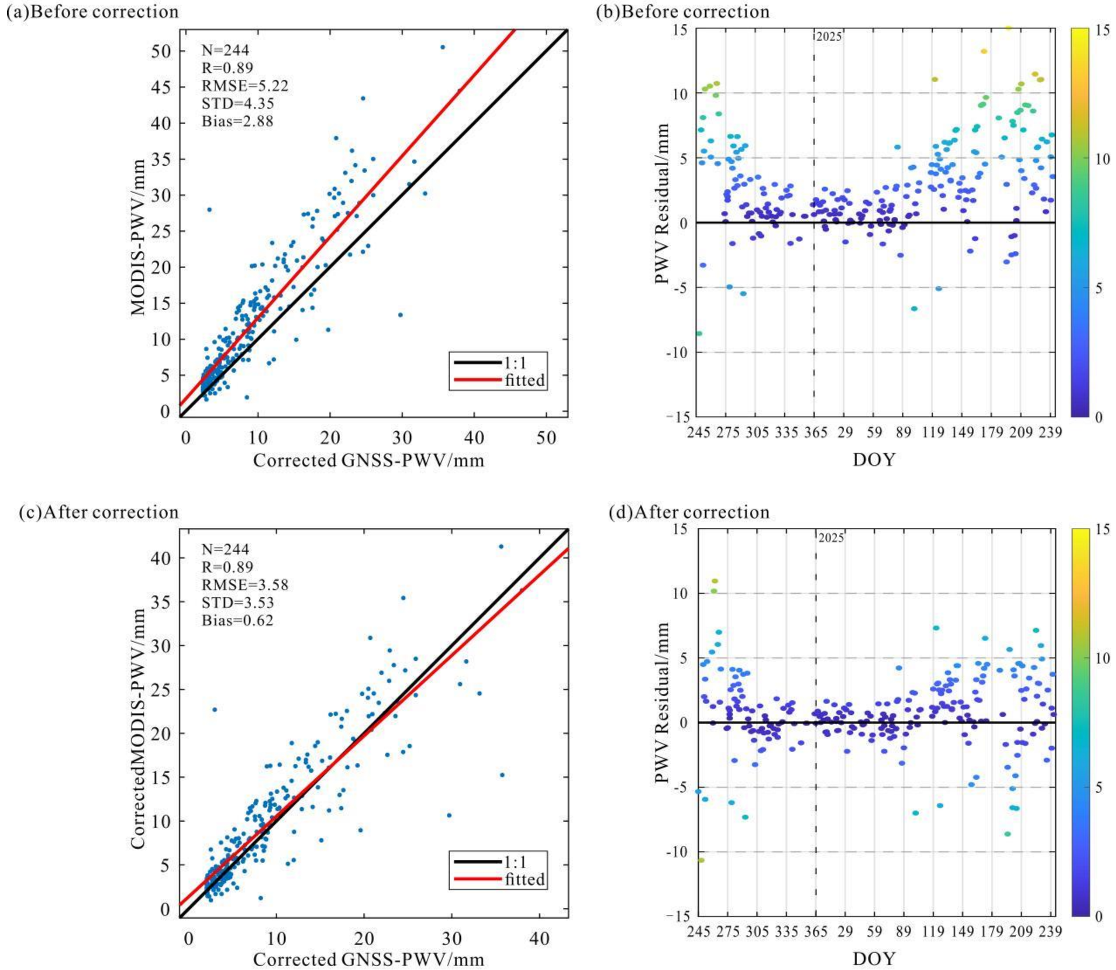

Figure 7: Comparison of MODIS-PWV with corrected GNSS-PWV at GSCM (Top) before and (Bottom) after applying the GSIA-derived linear correction: (Left) scatterplots and fitted lines and (Right) the corresponding residual time series.

4 Discussion

The results show that MODIS-PWV can capture the intra-annual variation in total column water vapor over the arid Hexi Corridor, but it exhibits an overestimation of approximately 2–3 mm across the entire study period, with larger errors during summer when atmospheric water vapor is relatively high. This positive bias has also been reported in previous evaluations of MODIS-PWV in various regions across China. Similar overestimation results are also found in other arid regions outside China (Khaniani et al., 2020). The error characteristics of MODIS-PWV are found to be closely related to regional atmospheric moisture background, seasonality, and the underlying surface environment (Lu et al., 2011; Zhu et al., 2021; Wang et al., 2017; Zhao et al., 2022).

Among the GNSS-PWV retrieval schemes examined in this study, PPP combined with integrated T_m was the most suitable option to be applied in the arid study region, although linear correction was still required. This result demonstrates the necessity of using ground-based RS-PWV observations to constrain GNSS-PWV, rather than directly using the uncorrected GNSS-PWV retrievals. The T_m estimation method had a marked influence on PPP-derived PWV, whereas GAMIT-derived PWV showed little difference between the integrated and empirical T_m schemes. Previous studies have identified the T_m model as a source of uncertainty in GNSS-PWV retrieval and shown that empirical T_m relationships are not strictly consistent across different regions or seasons (Wang et al., 2016; Sapucci, 2014). This is also verified in this study, suggesting that the Bevis empirical T_m equation may have limited applicability under arid and low-moisture conditions. The improvement produced by the integrated T_m was most evident for the PPP method, indicating that a physically based estimate of T_m is more effective than an empirical relationship in reducing outlying errors in arid regions.

Regarding the application conditions and error distribution of remotely sensed water vapor products, MODIS near-infrared PWV retrieval relies on ratios between water vapor absorption bands and atmospheric window bands, and the algorithm is applicable primarily under daytime and clear-sky conditions after removing the cloud-contaminated pixels. Although strict cloud-mask screening improves pixel purity, it also concentrates the available samples within a clear-sky subset, resulting in a smaller sample size and potential representativeness bias (Diedrich et al., 2015; Gao and Kaufman, 2003). Based on previous discussions of the error sources in MODIS-PWV retrieval, the increased dispersion observed during periods of relatively high atmospheric water vapor may result from the combined effects of residual thin clouds or sub-pixel cloud contamination, differences in surface albedo, and variations in observation geometry (Bai et al., 2021). In arid regions, the relatively homogeneous and stable underlying surface facilitates the integration of ground-based observations and multisource remote-sensing data to investigate both the causes of the overall MODIS-PWV overestimation and the spectral-response mechanisms associated with its reduced reliability under relatively high-water-vapor conditions. Such investigations represent an important direction for further improving the accuracy of MODIS-PWV retrievals in arid regions.

In terms of the correction methods for GNSS- and MODIS-PWV, the results show that univariate linear regression can substantially reduce the systematic bias of MODIS-PWV in the arid study region. This finding is consistent with Li et al. (2003), who applied a linear fitting model for MODIS-PWV correction and demonstrated that this method improved the agreement between MODIS-PWV and ground-based reference data derived from GPS and RS observations. Thus, for local evaluations with limited sample sizes, in which the main objective is to reduce systematic bias, the univariate linear regression is an appropriate correction method. More complex regional correction schemes or machine-learning methods may have greater potential for characterizing nonlinear errors (Xiong et al., 2021), but they place higher requirements on the size of the training dataset, the completeness of the explanatory variables, and cross-regional generalizability. Given the limited number of stations and the restricted observation period in the present study, a transparent and interpretable univariate linear correction is more appropriate under the current data conditions.

https://doi.org/10.5194/egusphere-2026-4722
Preprint. Discussion started: 2 September 2026

5 Conclusions

Based on observations from two GNSS stations in the arid Hexi Corridor, this study established a two-stage evaluation and correction method in which the RS observations were used to constrain GNSS-PWV, and the resulting GNSS-PWV was subsequently used to constrain MODIS-PWV. The main conclusions are as follows:

(1) The GNSS-PWV retrievals were sensitive to both the T_m estimation method and the GNSS processing strategy. Among the combination schemes examined, PPP combined with integrated T_m was more suitable for GNSS-PWV retrieval in arid regions. After correction using RS observations, the resulting PWV estimates achieved R = 0.97, RMSE = 2.30 mm, and Bias = 0.00 mm and could be used as a ground-based reference for the subsequent evaluation of MODIS-PWV.

(2) MODIS-PWV captured the intra-annual variation in column water vapor over the arid study region but showed an overall overestimation of approximately 2–3 mm. Relative to the corrected GNSS-PWV, the MODIS-PWV at the GSIA station yielded R = 0.97, RMSE = 3.47 mm, and Bias = 2.21 mm, whereas the corresponding values at GSCM were R = 0.89, RMSE = 5.22 mm, and Bias = 2.88 mm. These results indicate that MODIS-PWV can track variations in atmospheric water vapor, but its direct application to quantitative analyses in arid regions may overestimate water vapor content, particularly under high PWV conditions.

(3) The univariate linear correction model established using the corrected GNSS-PWV at GSIA substantially reduced the systematic bias of MODIS-PWV. At GSIA, the RMSE of MODIS-PWV relative to the corrected GNSS-PWV decreased from 3.47 to 2.05 mm. After accounting for the propagation of residual GNSS-PWV errors, Abs RMSE decreased from 4.16 to 3.08 mm, and Abs Bias decreased from 2.21 to 0.00 mm. When the correction equation was applied to GSCM, the RMSE relative to the corrected GNSS-PWV decreased from 5.22 to 3.58 mm, and Bias decreased from 2.88 to 0.62 mm. These results indicate that the linear correction relationship established using RS-constrained GNSS-PWV can improve the accuracy of MODIS-PWV in arid areas lacking radiosonde observations but equipped with GNSS stations.

This study was limited by the observation period and the number of stations and therefore could not fully cover the diversity of land-surface types across broader arid regions. Although the number of evaluation stations was limited, most existing station-network studies have directly used GNSS-PWV as the ground-based reference. The two-stage method proposed here, in which RS observations constrain GNSS-PWV and GNSS-PWV subsequently evaluate and correct MODIS-PWV, provides a more objective approach for evaluating remotely sensed water vapor products. Furthermore, the error magnitudes and biases quantified for a typical arid region, together with the resulting correction model, also provide a direct reference for the regional application of MODIS-PWV products in arid environments.

Code and data availability

The radiosonde observations are publicly available from the Department of Atmospheric Science at the University of Wyoming (https://weather.uwyo.edu/upperair/sounding.shtml). The ERA5 hourly data on single levels and pressure levels are available from the Copernicus Climate Data Store (Hersbach et al., 2018a, 2018b). The MOD05, MOD03, and MOD35 products are

https://doi.org/10.5194/egusphere-2026-4722
Preprint. Discussion started: 2 September 2026

available from the NASA LAADS DAAC (MODIS Atmosphere Science Team, 2017a, b; MODIS Science Data Support Team, 2017). The raw GNSS observations are not publicly available because their redistribution is restricted by the data provider.

Author contributions

JS and YW designed the study and developed the methodology. JS performed the data processing, software implementation, validation, formal analysis, data visualization, and preparation of the original manuscript. YW contributed to the methodology, validation, supervision, project administration, funding acquisition, and revision of the manuscript. YZ reviewed and edited the manuscript. ZL provided the GNSS observational resources and contributed to data curation. All authors approved the final manuscript.

Competing interests

The authors declare that they have no conflict of interest.

Acknowledgements

The authors thank the Department of Atmospheric Science at the University of Wyoming for providing public access to the radiosonde observations used in this study.

Financial support

This research has been supported by the National Natural Science Foundation of China (42171139, 42571162).

References

Allan, R. P. and Soden, B. J.: Atmospheric warming and the amplification of precipitation extremes, Science, 321, 1481–1484, https://doi.org/10.1126/science.1160787, 2008.

Bai, J., Lou, Y., Zhang, W., Zhou, Y., Zhang, Z., and Shi, C.: Assessment and calibration of MODIS precipitable water vapor products based on GPS network over China, Atmos. Res., 254, 105504, https://doi.org/10.1016/j.atmosres.2021.105504, 2021.

Bai, Q., Kong, Q., Mi, X., Chen, W., Ding, J., Huang, Y., Li, M., and Li, Q.: Evaluation and analysis of the precipitable water vapor in Inner Mongolia of China, Earth Planets Space, 77, 24, https://doi.org/10.1186/s40623-025-02157-1, 2025.

Bevis, M., Businger, S., Herring, T. A., Rocken, C., Anthes, R. A., and Ware, R. H.: GPS meteorology: Remote sensing of atmospheric water vapor using the Global Positioning System, J. Geophys. Res. Atmos., 97, 15787–15801, https://doi.org/10.1029/92JD01517, 1992.

https://doi.org/10.5194/egusphere-2026-4722
Preprint. Discussion started: 2 September 2026

Cui, J., Huang, Y. Z., Zhang, X. N., Ma, X. W., and Xu, S. A.: Evaluation of applicability of ERA5 data for GNSS precipitable water vapor retrieval in the Qinghai-Tibetan Plateau, J. Xi'an Univ. Sci. Technol., 45, 1243–1253, https://doi.org/10.13800/j.cnki.xakjdxxb.2025.0618, 2025.

Diedrich, H., Preusker, R., Lindstrot, R., and Fischer, J.: Retrieval of daytime total columnar water vapour from MODIS measurements over land surfaces, Atmos. Meas. Tech., 8, 823–836, https://doi.org/10.5194/amt-8-823-2015, 2015.

Ding, J., Chen, J., Tang, W., and Song, Z.: Spatial–temporal variability of global GNSS-derived precipitable water vapor (1994–2020) and climate implications, Remote Sens., 14, 3493, https://doi.org/10.3390/rs14143493, 2022.

Gao, B. C. and Goetz, A. F. H.: Column atmospheric water vapor and vegetation liquid water retrievals from airborne imaging spectrometer data, J. Geophys. Res. Atmos., 95, 3549–3564, https://doi.org/10.1029/JD095iD04p03549, 1990.

Gao, B. C. and Kaufman, Y. J.: Water vapor retrievals using Moderate Resolution Imaging Spectroradiometer (MODIS) near-infrared channels, J. Geophys. Res. Atmos., 108, 4389, https://doi.org/10.1029/2002JD003023, 2003.

Gao, B. C., Goetz, A. F. H., Westwater, E. R., Conel, J. E., and Green, R. O.: Possible near-IR channels for remote sensing precipitable water vapor from geostationary satellite platforms, J. Appl. Meteorol. Climatol., 32, 1791–1801, https://doi.org/10.1175/1520-0450(1993)032<1791:PNICFR>2.0.CO;2, 1993.

Ghaderi, M. and Rahimzadegan, M.: Improving precipitable water vapor estimations of the Moderate Resolution Imaging Spectroradiometer (MODIS) using metaheuristic algorithms, Adv. Space Res., 69, 4274–4287, https://doi.org/10.1016/j.asr.2022.03.035, 2022.

Held, I. M. and Soden, B. J.: Robust responses of the hydrological cycle to global warming, J. Clim., 19, 5686–5699, https://doi.org/10.1175/JCLI3990.1, 2006.

Hersbach, H., Bell, B., Berrisford, P., Biavati, G., Horányi, A., Muñoz Sabater, J., Nicolas, J., Peubey, C., Radu, R., Rozum, I., Schepers, D., Simmons, A., Soci, C., Dee, D., and Thépaut, J.-N.: ERA5 hourly data on single levels from 1940 to present, Copernicus Climate Change Service (C3S) Climate Data Store (CDS) [data set], https://doi.org/10.24381/cds.adbb2d47, 2018a.

Hersbach, H., Bell, B., Berrisford, P., Biavati, G., Horányi, A., Muñoz Sabater, J., Nicolas, J., Peubey, C., Radu, R., Rozum, I., Schepers, D., Simmons, A., Soci, C., Dee, D., and Thépaut, J.-N.: ERA5 hourly data on pressure levels from 1940 to present, Copernicus Climate Change Service (C3S) Climate Data Store (CDS) [data set], https://doi.org/10.24381/cds.bd0915c6, 2018b.

Kaufman, Y. J. and Gao, B. C.: Remote sensing of water vapor in the near IR from EOS/MODIS, IEEE Trans. Geosci. Remote Sens., 30, 871–884, https://doi.org/10.1109/36.175321, 1992.

Khaniani, A. S., Nikraftar, Z., and Zakeri, S.: Evaluation of MODIS near-IR water vapor product over Iran using ground-based GPS measurements, Atmos. Res., 231, 104657, https://doi.org/10.1016/j.atmosres.2019.104657, 2020.

Li, H., Wan, W., Ji, R., Li, G. Y., Chen, X. N., Zhu, S. Y., Liu, B. J., Xu, Y., Luo, Z. L., Wang, S. L., and Cui, Y. K.: Inspects and prospects of satellite remote sensing monitoring ability for land surface water in China, Natl. Remote Sens. Bull., 27, 1554–1573, https://doi.org/10.11834/jrs.20220576, 2023.

Li, Z., Muller, J.-P., and Cross, P.: Comparison of precipitable water vapor derived from radiosonde, GPS, and Moderate-Resolution Imaging Spectroradiometer measurements, J. Geophys. Res. Atmos., 108, 4651, https://doi.org/10.1029/2003JD003372, 2003.

Liu, C. Z. and Xia, J.: Some points view on detection and attribution of observed changes in hydrological cycle under global warming, Adv. Clim. Change Res., 6, 313–318, https://doi.org/10.3969/j.issn.1673-1719.2010.05.001, 2010.

Liu, J., Liang, H., Sun, Z., and Zhou, X.: Validation of the moderate-resolution imaging spectroradiometer precipitable water vapor product using measurements from GPS on the Tibetan Plateau, J. Geophys. Res. Atmos., 111, D14103, https://doi.org/10.1029/2005JD007028, 2006.

https://doi.org/10.5194/egusphere-2026-4722
Preprint. Discussion started: 2 September 2026

Liu, S. W., Zhang, C. L., Guo, X. F., Chu, Y. L., Ge, D. Q., and Fan, J. H.: Theoretical study for application of MODIS atmospheric water vapor retrieval to InSAR atmospheric correction, J. Remote Sens., 11, 367–372, https://doi.org/10.3321/j.issn:1007-4619.2007.03.011, 2007.

Liu, X. S., Ma, Z., Li, H. J., and Zhao, Q. Z.: Atmospheric water vapor retrieval algorithm integrating GNSS and remote sensing satellite, Sci. Surv. Mapp., 50, 25–32, https://doi.org/10.16251/j.cnki.1009-2307.2025.10.004, 2025.

Liu, Y., Zhang, W. Y., Li, W. Y., Zhang, S. B., Zhang, K. F., Wang, N. D., Gao, Y., and Wang, M. Y.: MODIS PWV neural network correction model considering spatial neighborhood characteristics, Natl. Remote Sens. Bull., 30, 144–155, https://doi.org/10.11834/jrs.20254201, 2026.

Lu, N., Qin, J., Yang, K., Gao, Y., Xu, X., and Koike, T.: On the use of GPS measurements for Moderate Resolution Imaging Spectrometer precipitable water vapor evaluation over southern Tibet, J. Geophys. Res. Atmos., 116, D23117, https://doi.org/10.1029/2011JD016160, 2011.

Luo, X., Wang, K., Jiang, H., Sun, J., and Zhu, Q.: Estimation of land surface evapotranspiration over the Heihe River basin based on the revised three-temperature model, Hydrol. Process., 26, 1263–1269, https://doi.org/10.1002/hyp.8182, 2012.

Miao, C., Sun, Q., Borthwick, A. G. L., and Duan, Q.: Linkage between hourly precipitation events and atmospheric temperature changes over China during the warm season, Sci. Rep., 6, 22543, https://doi.org/10.1038/srep22543, 2016.

MODIS Atmosphere Science Team: MODIS/Terra total precipitable water vapor 5-min L2 swath 1 km and 5 km, Collection 6.1, NASA Level-1 and Atmosphere Archive and Distribution System Distributed Active Archive Center (LAADS DAAC) [data set], https://doi.org/10.5067/MODIS/MOD05_L2.061, 2017a.

MODIS Atmosphere Science Team: MODIS/Terra cloud mask and spectral test results 5-min L2 swath 250 m and 1 km, Collection 6.1, NASA Level-1 and Atmosphere Archive and Distribution System Distributed Active Archive Center (LAADS DAAC) [data set], https://doi.org/10.5067/MODIS/MOD35_L2.061, 2017b.

MODIS Science Data Support Team: MODIS/Terra geolocation fields 5-min L1A swath 1 km, Collection 6.1, NASA Level-1 and Atmosphere Archive and Distribution System Distributed Active Archive Center (LAADS DAAC) [data set], https://doi.org/10.5067/MODIS/MOD03.061, 2017.

NASA/LARC/SD/ASDC: NASA Water Vapor Project MEaSUREs (NVAP-M) climate total precipitable water, version 1, NASA Langley Atmospheric Science Data Center [data set], https://doi.org/10.5067/NVAP-M/NVAP_CLIMATE_TOTAL-PRECIPITABLE-WATER_L3.001, 2013.

Saastamoinen, J.: Contributions to the theory of atmospheric refraction: Part II. Refraction corrections in satellite geodesy, Bull. Géod., 107, 13–34, https://doi.org/10.1007/BF02522083, 1973.

Sapucci, L. F.: Evaluation of modeling water-vapor-weighted mean tropospheric temperature for GNSS-integrated water vapor estimates in Brazil, J. Appl. Meteorol. Climatol., 53, 715–730, https://doi.org/10.1175/JAMC-D-13-048.1, 2014.

Shen, J.: Analysis of tropospheric delay and water vapor content using GPS during fog and haze, Master's thesis, Wuhan University, Wuhan, China, 2018.

Trenberth, K. E., Fasullo, J., and Smith, L.: Trends and variability in column-integrated atmospheric water vapor, Clim. Dyn., 24, 741–758, https://doi.org/10.1007/s00382-005-0017-4, 2005.

Wang, J., Zhang, L., Dai, A., Van Hove, T., and Van Baelen, J.: A near-global, 2-hourly data set of atmospheric precipitable water from ground-based GPS measurements, J. Geophys. Res. Atmos., 112, D11107, https://doi.org/10.1029/2006JD007529, 2007.

https://doi.org/10.5194/egusphere-2026-4722
Preprint. Discussion started: 2 September 2026

Wang, W. M., Sun, X. M., Zhang, R. H., Tang, X. Z., and Zhu, Z. L.: The simulation analyze of the effect of surface reflective spectrum on the retrieval of water vapor with MODIS NIR data, J. Remote Sens., 9, 8–15, https://doi.org/10.3321/j.issn:1007-4619.2005.01.002, 2005.

Wang, X., Zhang, K., Wu, S., Fan, S., and Cheng, Y.: Water vapor-weighted mean temperature and its impact on the determination of precipitable water vapor and its linear trend, J. Geophys. Res. Atmos., 121, 833–852, https://doi.org/10.1002/2015JD024181, 2016.

Wang, X. L.: Ground GNSS remote sensing for near-surface water environmental parameters, Doctoral dissertation, Chang'an University, Xi'an, China, 2018.

Wang, Y., Yang, K., Pan, Z., Qin, J., Chen, D., Lin, C., Chen, Y., Lazhu, Tang, W., Han, M., Lu, N., and Wu, H.: Evaluation of precipitable water vapor from four satellite products and four reanalysis datasets against GPS measurements on the southern Tibetan Plateau, J. Clim., 30, 5699–5713, https://doi.org/10.1175/JCLI-D-16-0630.1, 2017.

Wu, M., Jin, S., Li, Z., Cao, Y., Ping, F., and Tang, X.: High-precision GNSS PWV and its variation characteristics in China based on individual station meteorological data, Remote Sens., 13, 1296, https://doi.org/10.3390/rs13071296, 2021.

Xie, S., Zhang, J., Huang, L., Chen, F., Wu, Y., Wang, Y., and Liu, L.: A hybrid-grid global model for the estimation of atmospheric weighted mean temperature considering time-varying vertical adjustment rate in GNSS precipitable water vapour retrieval, Geosci. Model Dev., 18, 6987–7002, https://doi.org/10.5194/gmd-18-6987-2025, 2025.

Xiong, Z., Sun, X., Sang, J., and Wei, X.: Modify the accuracy of MODIS PWV in China: A performance comparison using random forest, generalized regression neural network and back-propagation neural network, Remote Sens., 13, 2215, https://doi.org/10.3390/rs13112215, 2021.

Xu, M. Z.: Construction of atmospheric water vapor field with high spatiotemporal resolution based on GNSS/MODIS multi-fusion data, Master's thesis, Shandong Jianzhu University, Jinan, China, 2022.

Yu, X., Zhao, G., Zhao, W., Yan, T., and Yuan, X.: Analysis of precipitation and drought data in Hexi Corridor, northwest China, Hydrology, 4, 29, https://doi.org/10.3390/hydrology4020029, 2017.

Zhang, W., Lou, Y., Cao, Y., Liang, H., Shi, C., Huang, J., Liu, W., Zhang, Y., and Fan, B.: Corrections of radiosonde-based precipitable water using ground-based GPS and applications on historical radiosonde data over China, J. Geophys. Res. Atmos., 124, 3208–3222, https://doi.org/10.1029/2018JD029662, 2019.

Zhang, Y., Fu, G., Sun, B., Zhang, S., and Men, B.: Simulation and classification of the impacts of projected climate change on flow regimes in the arid Hexi Corridor of northwest China, J. Geophys. Res. Atmos., 120, 7429–7453, https://doi.org/10.1002/2015JD023294, 2015.

Zhao, Q., Yao, Y., and Yao, W.: GPS-based PWV for precipitation forecasting and its application to a typhoon event, J. Atmos. Sol.-Terr. Phys., 167, 124–133, https://doi.org/10.1016/j.jastp.2017.11.013, 2018.

Zhao, Y., Zhao, H., Li, J., and Xiao, G.: Comprehensive validation and calibration of MODIS PWV over mainland China, Atmosphere, 13, 1763, https://doi.org/10.3390/atmos13111763, 2022.

Zheng, Z., Dong, W., Li, Z., Zhao, W., Hu, S., Yan, X., Zhao, J., and Wei, Z.: Observational study of surface spectral radiation and corresponding albedo over Gobi, desert, and bare loess surfaces in northwestern China, J. Geophys. Res. Atmos., 120, 883–896, https://doi.org/10.1002/2014JD022516, 2015.

Zhu, D., Zhang, K., Yang, L., Wu, S., and Li, L.: Evaluation and calibration of MODIS near-infrared precipitable water vapor over China using GNSS observations and ERA-5 reanalysis dataset, Remote Sens., 13, 2761, https://doi.org/10.3390/rs13142761, 2021.